Self-Sensing Design and Control for an Induction Machine with an Additional Short-Circuited Rotor Coil

Stefan Luecke* and Axel Mertens
Leibniz University Hannover
Institute for Drive Systems and Power Electronics
Welfengarten 1
Hanover, Germany
Phone: +49 (0) 511-762 2514
Fax: +49 (0) 511-762 3040
Email: stefan.luecke@stud.uni-hannover.de
URL: http://www.ial.uni-hannover.de

Acknowledgments

This work was funded by the Deutsche Forschungsgemeinschaft (DFG, German Research Foundation) – project identification number 424944120.

Keywords

≪Induction motor≫, ≪Design≫, ≪Impedance measurement≫, ≪Sensorless control≫

Abstract

In order to control an electrical machine at lower speeds, several control methods require a saliency. This paper presents an induction machine design to achieve a saliency for high frequency injection signals. The saliency is characterized for a prototype and a control method for the whole operation range is shown.

Introduction

Self-sensing control methods for induction machines (IMs) often use electromotive force (EMF)-based techniques in the medium and upper speed range and saliency-based methods applying a high frequency (HF) injection at low or zero speed. For the control, a certain level of saliency is required. However, IMs have a low saliency inherently. A machine design with good self-sensing ability is desired where other properties, like torque ripple, rated torque and efficiency remain unchanged. A demodulation technique applying a rotational HF injection is proposed in [1]. There, an IM design is used, which modulates the rotor slot leakage by changing the heights or widths of the slot openings. For this approach, a simulative design study concerning self-sensing and power conversion properties is done in [2]. Experimental results for prototypes with spatial modulation in the rotor slot opening height and width are shown in [3]. However, there is a trade off between self-sensing ability and power conversion, because the demands on the rotor slot opening design are opposed. An IM design using additional sensing windings on the stator is proposed in [4]. However, this approach requires additional terminals and an external excitation source. Another option for the enhancement of the saliency is the integration of an additional short-circuited coil in one axis of the rotor, which has been investigated for synchronous machine so far, e.g. in [5], [6], [7] and [8]. Thereby, the inductance is damped in this axis for high frequencies and thus,

*was an employee at the Institute for Drive Systems and Power Electronics from 2014 to 2019 and currently works at IAV GmbH.

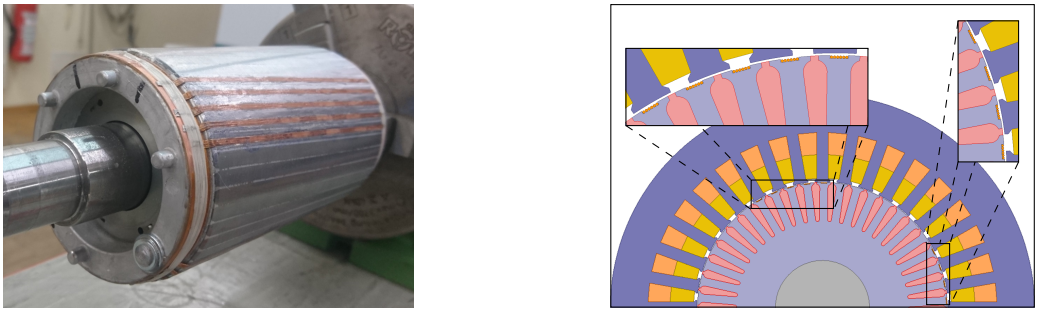

(a) Rotor with additional coil

(b) Schematic sketch

Fig. 1: Prototype with additional short-circuited rotor coil of a 4-pole, 1,5 kW IM

an inductive saliency occurs. In addition, the resistive saliency is amplified with this approach and the saliency enhancement has been experimentally validated, for instance in [8].

This paper evaluates the inductive saliency and the resistive saliency for an IM prototype with an additional short-circuited coil. Furthermore, a self-sensing control based on a flux observer structure and using a combined EMF-based and saliency-based evaluation is suggested.

Induction machine with an additional short-circuited rotor coil

The generation of a rotor-fixed saliency is based on the fact that a short-circuited winding damps a time-varying magnetic field, because the current, which is induced in the winding, counteracts the cause according to Lenz's law. If a winding is only placed in one axis of the rotor, the magnetic field is only damped in one axis. This leads to unequal effective inductances in the axes. The damping effect of the additional winding is frequency-dependent determined by its time constant, which is given by its inductance and resistance. Thus, the added rotor coil can be designed to be primarily effective in the high frequency range. The principle is described for this special rotor design in [9] in more detail. A prototype of a four-pole IM was built with four and five additional conductors per pole pitch. The additional slots are placed in the middle of the rotor teeth and the conductors are connected via two short-circuit rings at the rotor ends. A picture of the rotor and the cross section of the prototype's design are shown in Fig. 1a and Fig. 1b, respectively.

Impedance measurement

The saliency of the prototype is characterized using different methods. First, the impedance is measured with the impedance analyzer 6500B from Wayne Kerr and the network analyzer Bode100 from OMICRON LAB. During the measurement, the IM is at standstill and the measurement is repeated for several rotor positions. In Fig. 2 the results for a single frequency (here 2.5 kHz) and rotor positions covering one pole pair are shown. A β-excitation is applied using the setup shown in Fig. 2a. The inductance L_β and resistance R_β concerning this excitation over the mechanical rotor angle δ_R are presented in Fig. 2b and Fig. 2c. A variation of both quantities can be seen, which is caused by the additional coil. In order to evaluate the frequency behavior, Fig. 3 shows the inductance L_β and resistance R_β for selected rotor positions. With the impedance analyzer from Wayne Kerr and the network analyzer Bode100 the impedance can be measured down to 20 Hz and 1 Hz, respectively. It can be seen that the inductance depends on the rotor position. In addition, a reversal of the direction of the inductance difference can be noticed in the range from 300 to 700 Hz. The increase of the resistance with frequency results from the skin effect. In the range from around 1 to 3 kHz a clear spread of the resistance values can be observed, so that a high resistive saliency is present in this range. In order to characterize the inductive and resistive saliency, the salience ratios

$$S_L = \frac{L_\Delta}{L_\Sigma} \quad \text{and} \quad S_R = \frac{R_\Delta}{R_\Sigma} \tag{1}$$

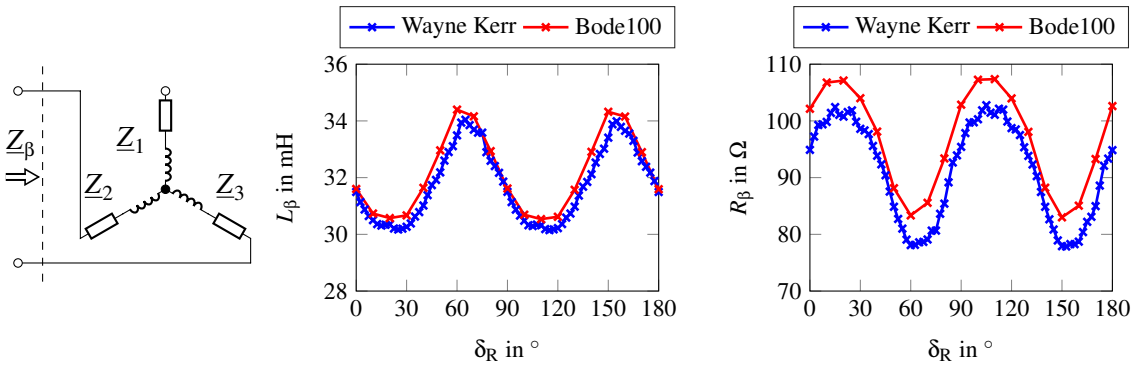

(a) β-excitation (b) Inductance (c) Resistance

Fig. 2: Impedance measurement: β-excitation setup (a), results obtained with the impedance analyzer (Wayne Kerr) and the network analyzer (Bode100) for the rotor position-dependent inductance (a) and resistance (b) at a frequency of 2.5 kHz

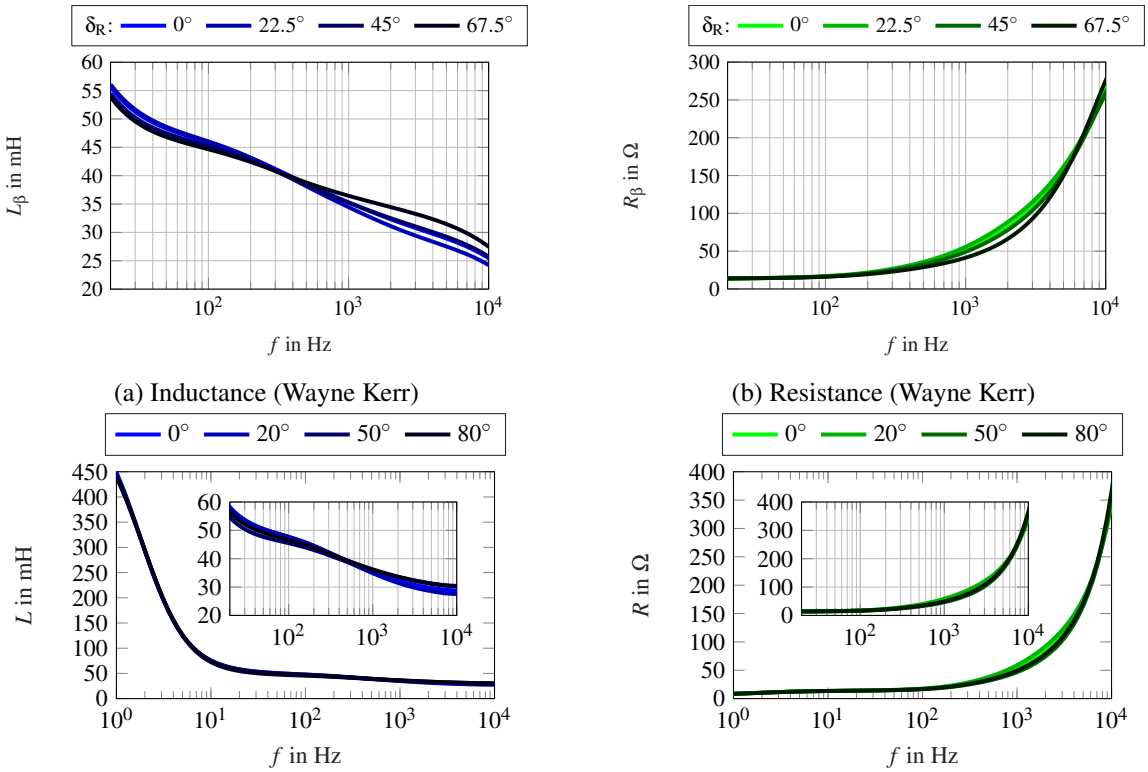

(a) Inductance (Wayne Kerr) (b) Resistance (Wayne Kerr)

(c) Inductance (Bode100) (d) Resistance (Bode100)

Fig. 3: Frequency dependency of the inductance (a)/(c) and the resistance (b)/(d) for certain rotor positions using the β-excitation setup, 1. row: measurement with the impedance analyzer form Wayne Kerr, 2. row: measurement with the network analyzer Bode100

are introduced, where L_Σ/R_Σ are the mean values of the inductance/resistance and L_Δ/R_Δ are the amplitudes of the 2th harmonic concerning one pole pair. Fig. 4 shows the behavior of S_L and S_R over frequency. A maximum inductive and resistive saliency of around 7 % and 16 % are reached, respectively. The following values are used to characterize the saliency behavior:

- The maximal saliency for low frequencies S_{LF}. This value is calculated by taking the maximum of S in a frequency range for 1 to 100 Hz.
- The maximal saliency for high frequencies S_{HF}. This value is calculated by taking the maximum of S in a frequency range above 100 Hz.

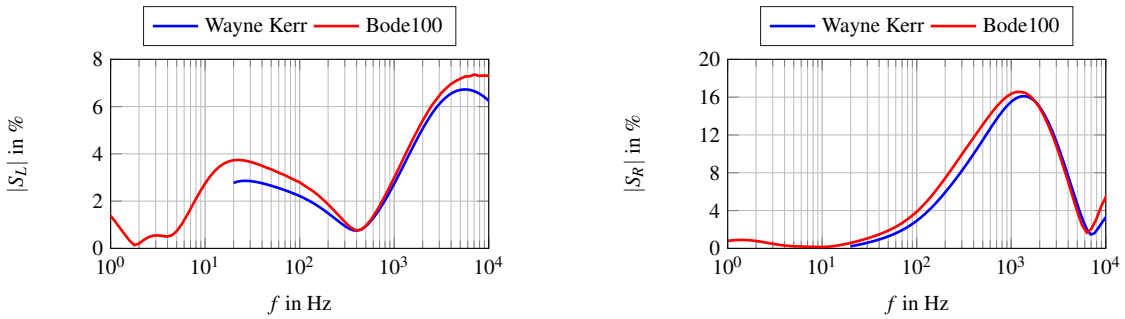

(a) Inductive saliency

(b) Resistive saliency

Fig. 4: Inductive saliency (a) and resistive saliency (b) over the frequency based on the impedance measurement

Table I: Comparison of characteristic saliency values

	S_{LF} in %	S_{HF} in %	$f_{S_{\mathrm{HF}}}$ in kHz
inductive (Wayne Kerr)	3.33	7.16	1.75
inductive (Bode 100)	3.92	7.47	1.94
resistive (Wayne Kerr)	2.88	16.50	0.50
resistive (Bode 100)	3.54	16.55	0.41

- The corner frequency of the HF saliency $f_{S_{\mathrm{HF}}}$. At this frequency the saliency value of $-3\,\mathrm{dB}$ (70.7 %) of S_{HF} is reached.

Table I summarizes the characteristic values obtained by the impedance measurement for the inductive and resistive saliency.

Measurement based on evaluation of current gradients

As a second method, the current gradients during a pulse width modulation (PWM) period are evaluated to determine the inductance matrix. The inverter, which supplies the IM, is operated with a constant duty cycle for one half bridge. The duty cycles of the other two half bridges remain zero. Thereby, different DC stator current levels with a certain current ripple due to the switching can be applied in the IM. The current during a PWM period can be divided into an active switching state (ASS) and a passive switching state (PSS). The following equations

$$\bar{\vec{u}}_{\mathrm{S,ASS},\alpha\beta} = R_{\mathrm{S}} \cdot \bar{\vec{i}}_{\mathrm{S,ASS},\alpha\beta} + \mathbf{L}^{\star}_{\sigma,\alpha\beta} \cdot \overline{\frac{\mathrm{d}}{\mathrm{d}t}\vec{i}}_{\mathrm{S,ASS},\alpha\beta} \quad \text{and} \tag{2}$$

$$\bar{\vec{u}}_{\mathrm{S,PSS},\alpha\beta} = R_{\mathrm{S}} \cdot \bar{\vec{i}}_{\mathrm{S,PSS},\alpha\beta} + \mathbf{L}^{\star}_{\sigma,\alpha\beta} \cdot \overline{\frac{\mathrm{d}}{\mathrm{d}t}\vec{i}}_{\mathrm{S,PSS},\alpha\beta}. \tag{3}$$

can be derived. The voltage due to the back EMF can be neglected, since the IM is operated at standstill and a DC current is applied. The bar over a magnitude denotes its average value during the respective switching state. The difference of (2) and (3)

$$\underbrace{\bar{\vec{u}}_{\mathrm{S,ASS},\alpha\beta} - \bar{\vec{u}}_{\mathrm{S,PSS},\alpha\beta}}_{\Delta\bar{\vec{u}}_{\alpha\beta}} = \mathbf{L}^{\star}_{\sigma,\alpha\beta} \cdot \underbrace{\left(\overline{\frac{\mathrm{d}}{\mathrm{d}t}\vec{i}}_{\mathrm{S,ASS},\alpha\beta} - \overline{\frac{\mathrm{d}}{\mathrm{d}t}\vec{i}}_{\mathrm{S,PSS},\alpha\beta} \right)}_{\Delta\overline{\frac{\mathrm{d}}{\mathrm{d}t}\vec{i}}_{\alpha\beta}}. \tag{4}$$

can be used to eliminate the resistance dependency. Finally, the inductance matrix can be calculated with

$$\mathbf{L}^{\star}_{\sigma,\alpha\beta} = \begin{pmatrix} \Delta\bar{\vec{u}}_{\alpha\beta,\mathrm{A1}} & \Delta\bar{\vec{u}}_{\alpha\beta,\mathrm{A2}} \end{pmatrix} \cdot \begin{pmatrix} \Delta\overline{\frac{\mathrm{d}}{\mathrm{d}t}\vec{i}}_{\alpha\beta,\mathrm{A1}} & \Delta\overline{\frac{\mathrm{d}}{\mathrm{d}t}\vec{i}}_{\alpha\beta,\mathrm{A2}} \end{pmatrix}^{-1} \tag{5}$$

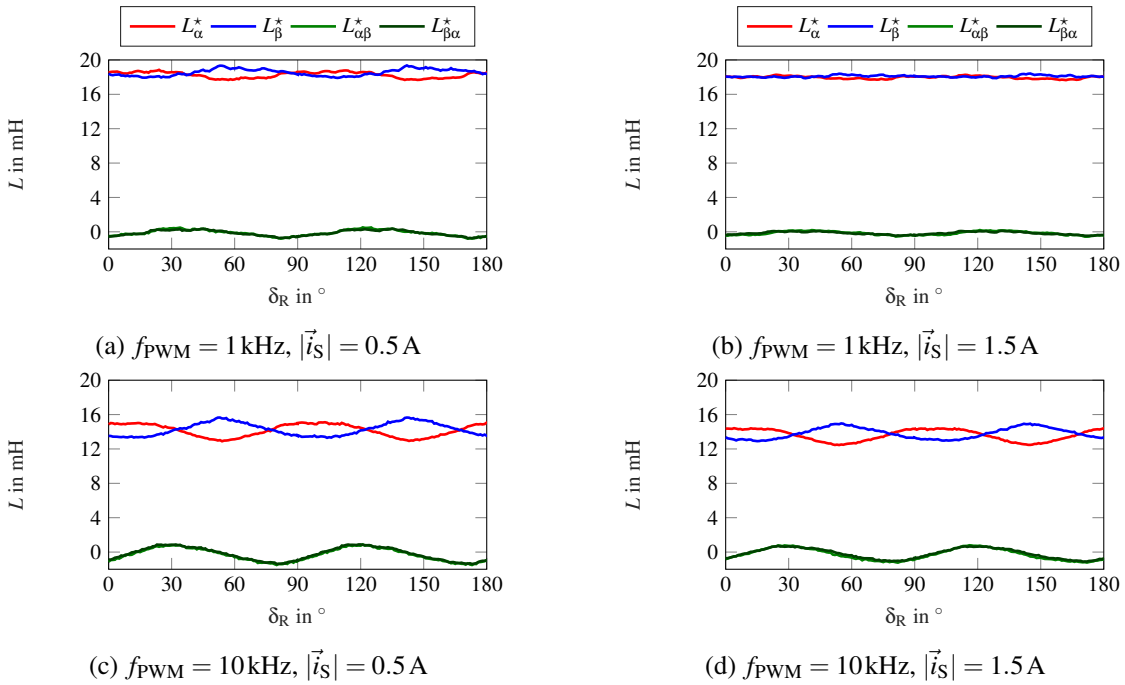

(a) $f_{\mathrm{PWM}} = 1\,\mathrm{kHz}$, $|\vec{i}_{\mathrm{S}}| = 0.5\,\mathrm{A}$

(b) $f_{\mathrm{PWM}} = 1\,\mathrm{kHz}$, $|\vec{i}_{\mathrm{S}}| = 1.5\,\mathrm{A}$

(c) $f_{\mathrm{PWM}} = 10\,\mathrm{kHz}$, $|\vec{i}_{\mathrm{S}}| = 0.5\,\mathrm{A}$

(d) $f_{\mathrm{PWM}} = 10\,\mathrm{kHz}$, $|\vec{i}_{\mathrm{S}}| = 1.5\,\mathrm{A}$

Fig. 5: Rotor position-dependent elements of $\mathbf{L}^\star_{\sigma,\alpha\beta}$ obtained at different switching frequencies f_{PWM} and stator current levels $|\vec{i}_{\mathrm{S}}|$

Table II: Inductive saliency values S_L obtained at different switching frequencies f_{PWM} and stator current levels $|\vec{i}_{\mathrm{S}}|$

$\lvert\vec{i}_{\mathrm{S}}\rvert$ \ f_{PWM}	1 kHz	2.5 kHz	5 kHz	10 kHz
0.5 A	2.57 %	5.59 %	6.76 %	7.09 %
1.5 A	1.02 %	4.42 %	6.39 %	6.87 %

by using two excitations A1 and A2. During A1 and A2 the first and second half bridge is switching, respectively. Fig. 5 shows the results for two different stator current levels and two switching frequencies. $L^\star_\alpha$, $L^\star_\beta$, $L^\star_{\alpha\beta}$ and $L^\star_{\beta\alpha}$ are the elements of $\mathbf{L}^\star_{\sigma,\alpha\beta}$. The rotor position is changed during the identification process in 1°-steps. The phase current and voltages are measured with the oscilloscope HD08108 from Lecroy. In order to get a better resolution for the current gradient evaluation, the DC link voltage is small. Table II summarizes the results of the inductive saliency obtained for four different frequencies. With a rising current level, the inductive saliency values S_L decreases. The saturation effect is more dominant at smaller frequencies, because at higher frequencies the effect of the additional rotor coil becomes stronger.

Comparison

The results obtained by the impedance measurement and the evaluation of the current gradients are compared in Table III for a frequency of 2.5 kHz. Such a value can be applied using a rotational or alternating HF injection. In order to compare the results for a similar IM operation condition, the value for $|\vec{i}_{\mathrm{S}}| = 0.5\,\mathrm{A}$ is used. Because of the β-excitation setup the measured inductances are twice as high as the inductances received by the second method. Therefore, the inductances obtained by the first method are divided by two for comparison reason. Regarding the maximal saliency for high frequencies S_{HF}, the values 7.16 %, 7.47 % and 7.09 % are obtained. The values match well.

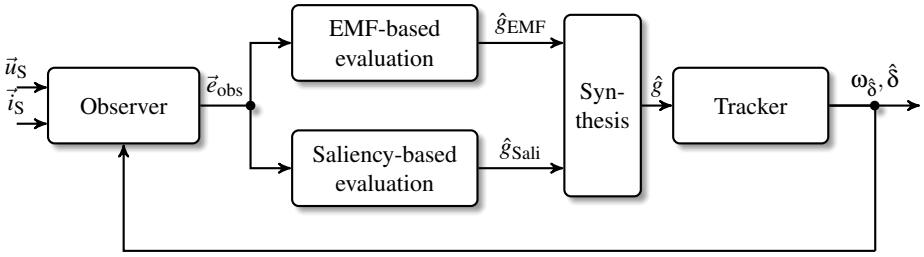

Fig. 6: Block diagram of rotor speed and position estimation method for the proposed self-sensing control

Self-sensing control method for the whole operation range

A self-sensing control method for the IM based on the gradient descent method is suggested, which is capable to operate the IM in the complete speed range. The basic block diagram of the electrical rotor angle and the rotor angle velocity estimation is shown in Fig. 6. The key features are the observer (Fig. 7a) and the two evaluations which calculate the gradients based on the EMF and the saliency (Fig. 7b and Fig. 7c). Further, the tracker consists of a PI controller and an integrator. The gradients are combined depending on three speed intervals. If the absolute speed is below the limit n_{Sali}, the saliency-based evaluation is active. If the absolute speed is above the limit n_{EMF}, the EMF-based evaluation is active and in between these limits the gradients are weighted linearly. An arbitrary HF injection is needed if the saliency-based evaluation is active at low speed. A similar control method is used for the synchronous machine in [10].

The self-sensing control is tested at two test stands. Test stand A has a 20 kW, six-pole IM with no additional short-circuited rotor coil and test stand B includes a 1.5 kW, four-pole IM with an additional short-circuited rotor coil. Fig. 8a shows a reference speed step from 1500 rpm to 1600 rpm obtained at test stand A at rated torque while the EMF-based evaluation is active. Low-frequency oscillation can be

Table III: Comparison of the results of the impedance measurement and evaluation of the current gradients for the frequency 2.5 kHz

Method	L_Σ in mH	L_Δ in mH	S_L in %
Impedance measurement (Wayne Kerr)	15.9	0.97	6.09
Impedance measurement (Bode 100)	16.1	0.95	5.93
Current gradient	16.0	0.90	5.59

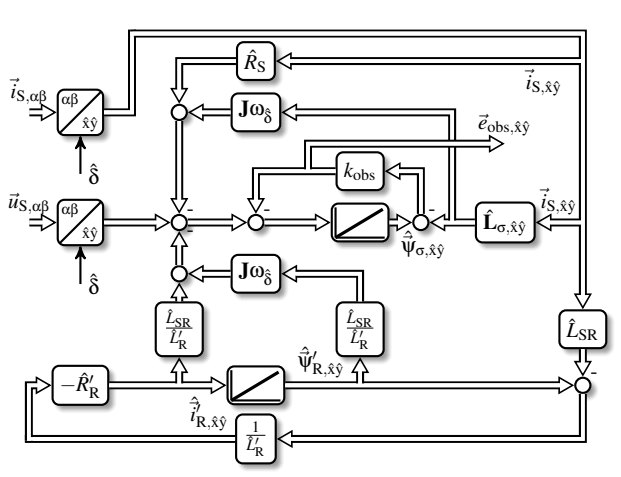

(a) Observer

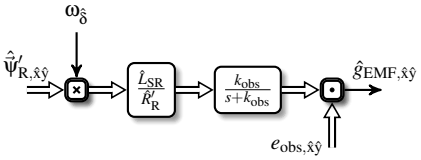

(b) EMF-based evaluation

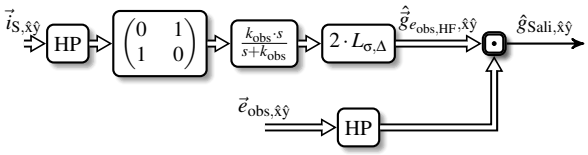

(c) Saliency-based evaluation

Fig. 7: Block diagrams of key features of the proposed estimation

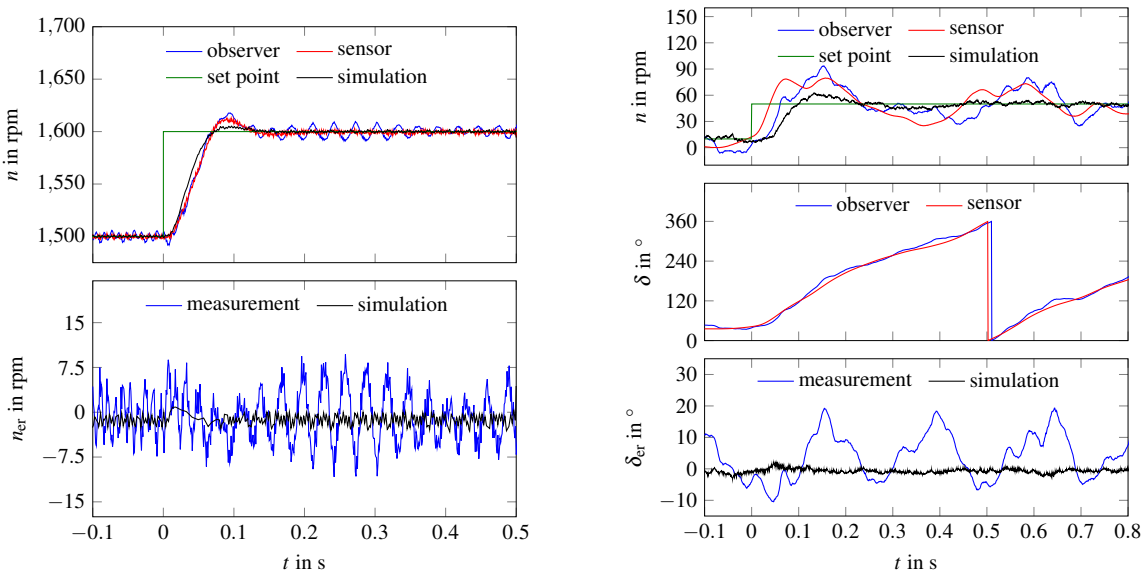

(a) $T = 27\,\mathrm{Nm}$ (b) $T = 7.5\,\mathrm{Nm}$, $f_{\mathrm{HF}} = 2.5\,\mathrm{kHz}$, $\hat{i}_{\mathrm{HF}} = 0.2\,\mathrm{A}$

Fig. 8: Measurement results and comparison with simulation for self-sensing speed control for different speed ranges using the EMF-based evaluation at test stand A (a) and using saliency-based evaluation at test stand B (b)

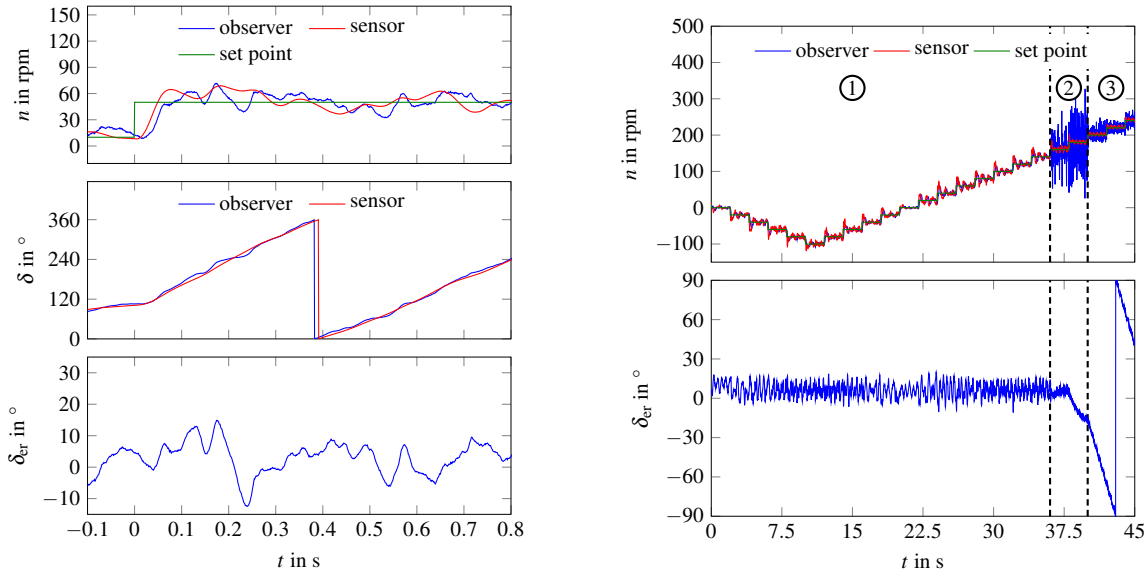

(a) $T = 5\,\mathrm{Nm}$, $f_{\mathrm{HF}} = 2.5\,\mathrm{kHz}$, $\hat{i}_{\mathrm{HF}} = 0.2\,\mathrm{A}$ (b) $T = 4\,\mathrm{Nm}$, $n_{\mathrm{Sali}} = 150\,\mathrm{rpm}$, $n_{\mathrm{EMF}} = 200\,\mathrm{rpm}$

Fig. 9: Measurement results for self-sensing speed control at test stand B using the saliency-based evaluation (a) and using the EMF- or/and saliency-based evaluation, respectively (b)

noticed on the speed error n_{er}. However, the mean value of the speed error is close to zero. The simulation forecasts the speed dynamic well. The overshoot is higher than predicted. A reference speed step from 10 rpm to 50 rpm is shown in Fig. 8b. The waveforms are obtained at test stand B at a torque of 7.5 Nm (75 % of the rated torque) during the saliency-based evaluation is active. The speed follows the reference value. However, significant oscillations can be seen on the speed. The root cause is the oscillating rotor angle estimation error. The oscillations are not visible in the simulation. In order to evaluate the results, it has to be considered that the saliency is in the range of 6 % at the used injection frequency of 2.5 kHz. This is not a high value for a saliency-based self-sensing control. Further, the saturation has a negative effect. Appling a smaller torque, the control performance becomes better shown in Fig. 9a.

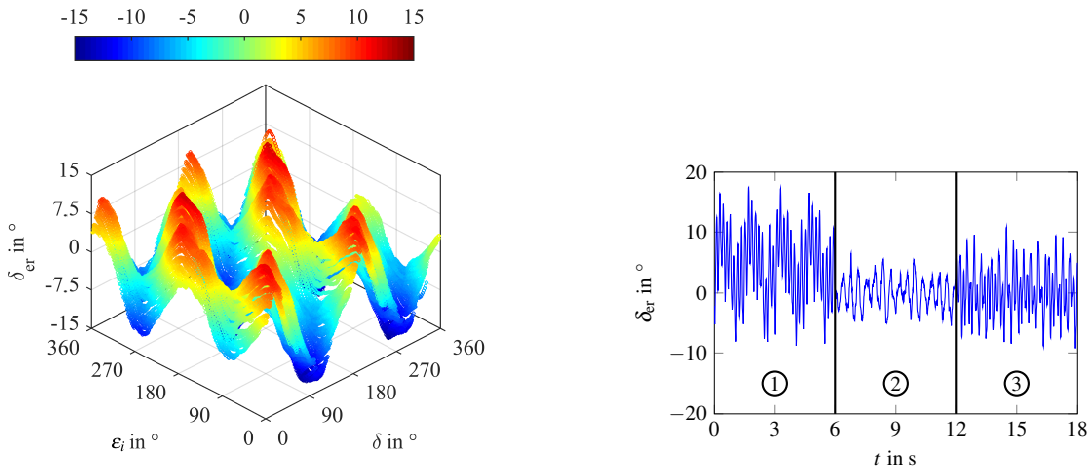

(a) $i_{S,d,set} = 2\,A$, $i_{S,q,set} = 3\,A$

(b) $i_{S,d,set} = 2\,A$, $i_{S,q,set} = 3\,A$

Fig. 10: Rotor angle estimation error identification depending on electrical rotor angle δ and the angle of the stator current space vector ε_i (a) and experimental results for rotor angle estimation error compensation obtained during current control operation (1: no compensation, 2: indirect compensation, 3: direct compensation)

Fig. 9b shows the experimental results, in which all speed ranges used for the synthesis of the gradients are passed through. The waveforms are obtained at a torque of 4 Nm. The performance of the speed control is degraded in the interval, in which both evaluations are active. In this range, the HF injection cannot be disabled, since the saliency-based evaluation is active. However, the HF injection disturbs the EMF-based evaluation. In order to identify the rotor angle estimation error, the IM is operated in current control mode using a speed sensor, the load machine is speed-controlled and the rotor angle estimation runs is active. Fig. 10a shows identified rotor angle estimation error. Two maxima exist over one electrical period of the rotor angle and the angle of stator current space vector. Two compensation methods are applied to reduce the rotor angle estimation error. The rotor angle can be corrected after the estimation (indirect compensation) or the rotor angle, which is fed back to the observer, is directly corrected within the estimation (direct compensation). Fig. 10b shows the experimental results for the compensation. The IM is operated with a speed sensor in order to avoid an interaction of self-sensing control on the estimation.

Conclusion

A modified rotor design with an additional short-circuited coil is proposed. The effect of the additional coil on the impedance and resistance is evaluated using two measurement techniques. For the investigated prototype, a maximal inductive saliency of around 7 % is achieved. The maximal resistive saliency is around 16 %. Further, a self-sensing control for the whole operation range using a EMF- and a saliency-based evaluation is suggested. Simulation and experimental results demonstrate the validity of the proposed method.

References

[1] Jansen P. L. and Lorenz R. D.: Transducerless position and velocity estimation in induction and salient AC machines, IEEE Trans. Ind. Appl. Vol. 31 no. 2, pp. 240-247, 1995

[2] Brown I. P. and Lorenz R. D.: Induction machine design methodology for self-sensing: Balancing saliencies and power conversion properties, IEEE Trans. Ind. Appl. Vol. 47 no. 1, pp. 79-87, 2011

[3] Mingardi D., Bianchi N., Alberti L., and Zeni R.: Analysis and test of the sensorless capability of induction motors with created saliency, IEEE Trans. Ind. Appl. Vol. 52, no. 3, pp. 2186-2193, 2016

[4] Joy M. T. and Bcker J.: Sensorless control of induction motor drives using additional windings on the stator, IEEE 9th International Symposium on Sensorless Control for Electrical Drives (SLED), pp. 162-167, 2018

[5] Faggion A. , Bianchi N. , and Bolognani S.: Ringed-pole permanent-magnet synchronous motor for position sensorless drives, IEEE Trans. Ind. Appl. Vol. 47 no. 4, pp. 1759-1766, 2011
[6] Graus J. and Hahn I.: Modelling and optimization of a short-circuited rotor winding of a PMSM for saliency tracking, 5th International Symposium on Sensorless Control for Electrical Drives (SLED), 2014
[7] Quattrone F. and Ponick B.: Active differential inductance control of permanent magnet synchronous machines using short-circuited rotor coils, IEEE Vehicle Power and Propulsion Conference (VPPC), 2015.
[8] Quattrone F. and Ponick B.: Evaluation of a permanent magnet synchronous machine with a rotor coil for improved self-sensing performance at low speed, XXII International Conference on Electrical Machines (ICEM), pp. 1680-1685, 2016
[9] Luecke S. and Mertens A.: Self-sensing control of induction machines using an additional short-circuited rotor coil, IEEE International Symposium on Sensorless Control for Electrical Drives (SLED), 2017
[10] Wiedmann K. and Mertens A.: Self-sensing control of PM synchronous machines including online system identification based on a novel mras approach, 3rd IEEE International Symposium on Sensorless Control for Electrical Drives (SLED), 2012